

Microscopic characterization of the magnetic properties of the itinerant antiferromagnet La_2Ni_7 by ^{139}La NMR/NQR measurements

Q.-P. Ding,¹ J. Babu,^{1,2} K. Rana,¹ Y. Lee,¹ S. L. Bud'ko,^{1,2} R. A. Ribeiro,^{1,2} P. C. Canfield,^{1,2} and Y. Furukawa^{1,2}

¹Ames National Laboratory, U.S. DOE, Ames, Iowa 50011, USA

²Department of Physics and Astronomy, Iowa State University, Ames, Iowa 50011, USA

(Dated: April 7, 2023)

^{139}La nuclear magnetic resonance (NMR) and nuclear quadrupole resonance (NQR) measurements have been performed to investigate the magnetic properties of the itinerant magnet La_2Ni_7 which shows a series of antiferromagnetic (AFM) phase transitions at $T_{\text{N}1} = 61$ K, $T_{\text{N}2} = 56$ K, and $T_{\text{N}3} = 42$ K under zero magnetic field. Two distinct La NMR signals were observed due to the two crystallographically inequivalent La sites in La_2Ni_7 (La1 and La2 in the La_2Ni_4 and the LaNi_5 sub-units of the La_2Ni_7 unit cell, respectively). From the ^{139}La NQR spectrum in the AFM state below $T_{\text{N}3}$, the AFM state was revealed to be a commensurate state where Ni ordered moments align along the crystalline c axis. Owing to the two different La sites, we were able to estimate the average values of the Ni ordered moments (~ 0.07 - $0.08 \mu_{\text{B}}/\text{Ni}$ and $\sim 0.17 \mu_{\text{B}}/\text{Ni}$ around La1 and La2, respectively) from ^{139}La NMR spectrum measurements in the AFM state below $T_{\text{N}3}$, suggesting a non-uniform distribution of the Ni-ordered moments in the AFM state. In contrast, a more uniform distribution of the Ni-ordered moments in the saturated paramagnetic state induced by the application of high magnetic fields is observed. The temperature dependence of the sublattice magnetization measured by the internal field at the La2 site in the AFM state was reproduced by a local moment model better than the self-consistent renormalization (SCR) theory for weak itinerant antiferromagnets. Given the small Ni-ordered moments in the magnetically ordered state, our results suggest that La_2Ni_7 has characteristics of both itinerant and localized natures in its magnetism. With this in mind, it is noteworthy that the temperature dependence of nuclear spin-relaxation rates ($1/T_1$) in the paramagnetic state above $T_{\text{N}1}$ measured at zero magnetic field can be explained qualitatively by both the SCR theory and the local-moment model.

I. INTRODUCTION

Fragile magnets with small ordered moments, such as weak itinerant ferromagnets and antiferromagnets, have attracted much interest in studying quantum phase transition since the magnetic states of those compounds can be tuned by perturbations such as magnetic field, pressure, and doping [1, 2]. As a part of our research projects on fragile magnets, we have recently been studying the itinerant antiferromagnet La_2Ni_7 in detail by using single crystals [3–5]. La_2Ni_7 crystallizes in a Ce_2Ni_7 type hexagonal structure (space group $P6_3/mmc$) [6, 7] and the lattice parameters are $a = b = 5.06235(11)$ Å and $c = 24.6908(8)$ Å at room temperature [3]. As shown in Fig. 1(a) [8], the structure consists of La_2Ni_4 and LaNi_5 sub-units and the unit cell contains two blocks of $[\text{La}_2\text{Ni}_4 + 2 \text{LaNi}_5]$ where two different La sites (La1 and La2 in the La_2Ni_4 and the LaNi_5 sub-units of the La_2Ni_7 unit cell, respectively) and five different sites for Ni atoms exist [9, 10]. The magnetic properties of the compound La_2Ni_7 have been investigated since the 1980's, but only in polycrystalline form. Magnetic susceptibility $\chi(T)$ measurements on La_2Ni_7 in polycrystalline samples show a maximum around 51-54 K corresponding to an antiferromagnetic (AFM) phase transition [11–13]. The effective moment and Curie-Weiss temperature in the paramagnetic state estimated from the $\chi(T)$ measurement were reported to be $0.80 \mu_{\text{B}}/\text{Ni}$ and 67 K, respectively [14]. The saturation moment of Ni ions in the magnetically ordered state was reported to be $\sim 0.08 \mu_{\text{B}}/\text{Ni}$ from

magnetization curves [15], which show the temperature-dependent metamagnetic behaviors, suggesting the existence of several magnetic phases [14, 16].

In fact, from the recent detailed specific heat, magnetization, and electrical resistivity measurements on single crystals, Ribeiro *et al.* [3] reported the complete, anisotropic magnetic field (H) - temperature (T) phase diagrams for the magnetic fields applied parallel and perpendicular to the crystallographic c axis shown in Fig. 1(c). In zero applied magnetic field, there are a series of antiferromagnetic (AFM) phase transitions at $T_{\text{N}1} \sim 61$ K, $T_{\text{N}2} \sim 56.5$ K, and $T_{\text{N}3} \sim 42$ K, making three different magnetically ordered phases named C, B, and A phases for $T_{\text{N}2} < T < T_{\text{N}1}$, $T_{\text{N}3} < T < T_{\text{N}2}$, and $T < T_{\text{N}3}$, respectively. It is noted that in the case of C phase, a small ferromagnetic (FM) component was reported in its AFM ordering [3]. Recent neutron diffraction (ND) measurements using single crystals indicate that the B and C phases are incommensurate AFM states where the ordered moments are perpendicular to the c axis in the C phase while an additional parallel component of the ordered moments along the c axis also exist in the B phase, and the A phase is commensurate where the ordered moments are parallel to the c axis [4]. The commensurate AFM state in the lowest temperature A phase reported by the ND measurements is consistent with the theoretical prediction [10] where two ferromagnetic unit blocks with opposite Ni spin directions are separated by the non-magnetic Ni layers in the La_2Ni_4 units; the Ni ordered moments are proposed to point the c axis and its magni-

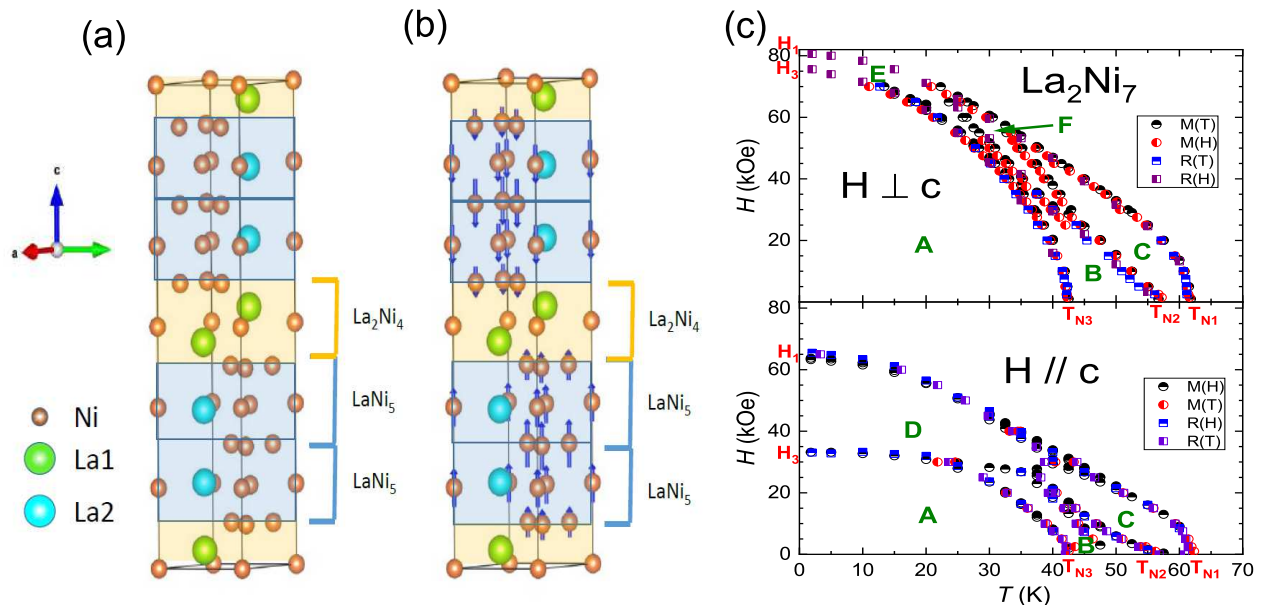


FIG. 1: (a) Crystal structure of La_2Ni_7 (space group $P6_3/mmc$) which consists of La_2Ni_4 and LaNi_5 sub-units with two different La sites (La1 and La2 in the La_2Ni_4 and the LaNi_5 sub-units, respectively). (b) Schematic view of spin distribution in the antiferromagnetic state (A phase) proposed by DFT calculations [10] and ND measurements [4]. (c) $H-T$ phase diagrams for $H \parallel c$ (bottom) and $H \perp c$ (top) reported by Ribeiro *et al.* based on the H and T dependences of magnetization [$M(H)$ and $M(T)$] and resistivity [$R(H)$ and $R(T)$] measurements [3].

tude depends on the Ni positions with minimum in the La_2Ni_4 sub-units and maximum at the middle of the two LaNi_5 sub-units as shown in Fig 1(b)) [10].

Although detailed studies of the thermodynamic, transport, and structural measurements on La_2Ni_7 using a single crystal have been performed, further studies such as the microscopic characterization of the static and dynamic magnetic properties would provide important information for characterizing the itinerant antiferromagnet La_2Ni_7 . Nuclear magnetic resonance (NMR) and nuclear quadrupole resonance (NQR) are powerful techniques to investigate the magnetic properties of materials from a microscopic point of view [17]. In particular, one can obtain direct and local information of the magnetic state at nuclear sites, helping to determine the magnetic structure of magnetic systems. In addition, the nuclear spin-lattice relaxation time, T_1 , provides important information about magnetic fluctuations.

Here we report the results of ^{139}La NMR and NQR measurements on La_2Ni_7 single crystals and oriented powder samples. Two distinct La signals with two different values of quadrupolar frequencies of $\nu_Q \sim 0.7$ and ~ 3.6 MHz are observed. Those are assigned to La1 and La2, respectively, based on density functional theory (DFT) calculations. In the antiferromagnetic state of the lowest temperature A phase, the internal magnetic induction B_{int} at La2 was directly determined to be -0.79 T at 4.2 K by the observation of the splitting of NQR lines. In addition, the direction of the B_{int} is deter-

mined to be parallel to the c axis from further splittings of NQR lines under small magnetic fields using a single crystal. From NMR measurements using oriented powder sample, we found the B_{int} values at La1 and La2 are close to $-(0.31-0.37)$ T and -0.75 T at 4.2 K, respectively, in the antiferromagnetic A phase. This result indicates that the Ni-ordered moments are not uniform and the average magnitude of Ni-ordered moments around La2 is greater than that around La1, which is consistent with the ND results and the DFT calculations. In further measurements, in a saturated paramagnetic state under a high magnetic field of 8 T parallel to the c axis at 4.3 K, B_{int} at La1 is found to increase to -0.48 T while B_{int} at La2 decreases to -0.37 T. These results suggest that Ni-ordered moments are more uniformly distributed in Ni positions in the saturated paramagnetic state. The temperature dependence of B_{int} at the La2 site was well reproduced by the localized moment model rather than the self-consistent renormalization (SCR) theory for weak itinerant antiferromagnets. The temperature dependence of $1/T_1$ measured at zero magnetic field in the paramagnetic state above T_{N1} can be reproduced by both the SCR theory and the localized moment model. These results suggest that the itinerant antiferromagnet La_2Ni_7 has magnetic properties characterized by localized moment nature, as well as the nature of weak itinerant antiferromagnets as seen by the small Ni-ordered moments in La_2Ni_7 .

II. EXPERIMENT

Hexagonal-shaped plate-like La_2Ni_7 single crystals were grown from high-temperature solutions as detailed in Ref. [3]. The crystalline c axis is perpendicular to the plane. NMR and NQR measurements of ^{139}La nuclei ($I = 7/2$, $\gamma_N/2\pi = 6.0146$ MHz/T, $Q = 0.21$ barns) were carried out using a lab-built phase-coherent spin-echo pulse spectrometer. The ^{139}La -NMR spectra were obtained by recording the integrated spin-echo intensity with changing H at a fixed frequency or changing resonance frequency at a constant magnetic field. The ^{139}La -NQR spectra in zero magnetic field were measured either by measuring the intensity of the Hahn spin echo in steps of frequency or performing the Fourier transform (FT) of the spin echo signals. For most of NMR/NQR measurements, we performed the measurements using powdered samples crushed from the single crystals, as the intensities of NMR/NQR signals for the single crystals are very weak, making the measurements difficult at higher temperatures. For NMR measurements, we used a loosely packed powder sample and found that the grains of loosely packed samples orient under magnetic fields and the orientation direction depends on temperature and magnetic field as shown below. Only for NQR measurements at the lowest temperature of $T = 1.6$ K under small magnetic fields, a single crystal was used to determine the internal field direction.

The ^{139}La spin-lattice relaxation rates ($1/T_1$) were measured using a saturation recovery method. $1/T_1$ at each temperature for an NQR line (corresponding to a transition line for $m = \pm 5/2 \leftrightarrow \pm 7/2$) was determined by fitting the nuclear magnetization (M) versus time (t) using the exponential function $1 - M(t)/M(\infty) = 0.214e^{-3t/T_1} + 0.649e^{-10t/T_1} + 0.136e^{-21t/T_1}$, where $M(t)$ and $M(\infty)$ are the nuclear magnetization at time t after the saturation and the equilibrium nuclear magnetization at $t \rightarrow \infty$, respectively [18].

III. RESULTS AND DISCUSSION

A. ^{139}La NMR in the paramagnetic state

Figure 2(a) shows the temperature (T) dependence of frequency-swept ^{139}La -NMR spectra for the loosely packed powder sample under a magnetic field of $H = 7.4089$ T. The typical spectrum for a nucleus with spin $I = 7/2$ with Zeeman and quadrupolar interactions can be described by a nuclear spin Hamiltonian [19]

$$\mathcal{H} = -\gamma_N \hbar (1 + K) \mathbf{H} \cdot \mathbf{I} + \frac{h\nu_Q}{6} (3I_z^2 - I^2), \quad (1)$$

where H is external field, \hbar is Planck's constant (h) divided by 2π , and K represents the NMR shift. The first and second terms represent Zeeman and quadrupolar interactions, respectively [20]. The nuclear quadrupole frequency for $I = 7/2$ nuclei is given by $\nu_Q = eQV_{ZZ}/14h$,

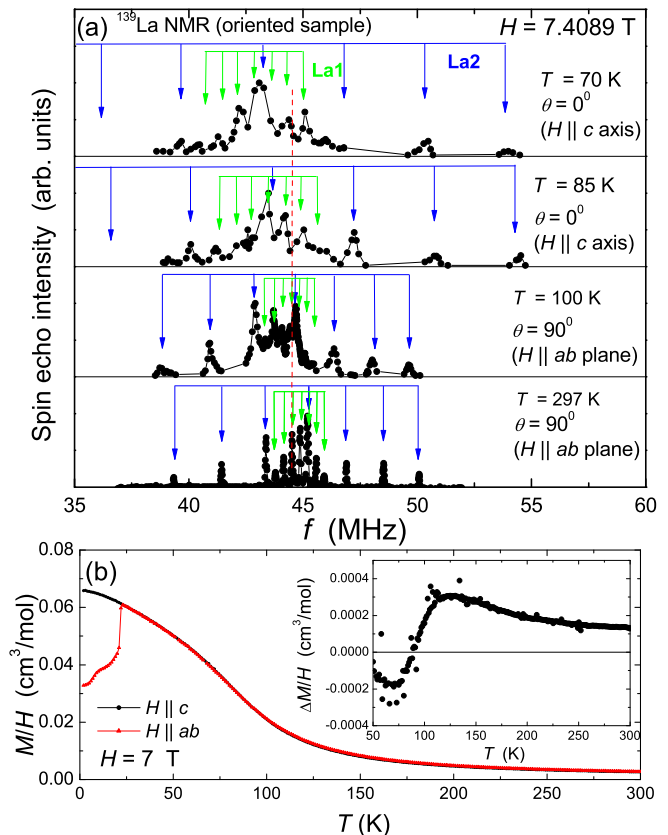


FIG. 2: (a) Frequency-swept ^{139}La -NMR spectra under $H = 7.4089$ T at various temperatures. The green and blue lines are the position of ^{139}La -NMR spectra calculated with a temperature independent $\nu_Q = 0.7$ MHz for La1 and $\nu_Q = 3.6$ MHz for La2, respectively. The vertical dashed red line corresponds to the Larmor magnetic field position. (b) Temperature dependence of M/H measured at $H = 7$ T parallel to the c axis [$(M/H)_c$ in black] and parallel to the ab plane [$(M/H)_{ab}$ in red]. The inset shows the temperature dependence of $\Delta M/H = (M/H)_{ab} - (M/H)_c$.

where Q is the nuclear quadrupole moment and V_{ZZ} is the maximum electric field gradient (EFG) at the nuclear site. In first-order perturbation theory, when the Zeeman interaction is much greater than the quadrupole interaction, one has the nuclear energy levels for $I = 7/2$

$$E_m = -\gamma_N \hbar (1 + K) H m - \frac{h\nu_Q}{12} (3 \cos^2 \theta - 1) (3m^2 - \frac{63}{4}), \quad (2)$$

where θ is the angle between the external magnetic field and the principal axis of the EFG. Thus ^{139}La NMR spectrum is composed of a central transition line and three pairs of satellite lines shifted from the central transition line by $\pm \frac{1}{2} \nu_Q (3 \cos^2 \theta - 1)$ (for the transitions of $m = 3/2 \leftrightarrow 1/2$ and $-3/2 \leftrightarrow -1/2$), $\pm \nu_Q (3 \cos^2 \theta - 1)$ (for $m = 5/2 \leftrightarrow 3/2$ and $-5/2 \leftrightarrow -3/2$), and $\pm \frac{3}{2} \nu_Q (3 \cos^2 \theta - 1)$ (for $m = 7/2 \leftrightarrow 5/2$ and $-7/2 \leftrightarrow -5/2$). It is noted that the spacing between the lines of the spectrum for $\theta = 0$ is twice that for $\theta = 90^\circ$, producing the spectrum for θ

= 0 almost two times wider than for $\theta = 90^\circ$.

As shown in Fig. 1(a), La_2Ni_7 has two inequivalent La sites: La1 and La2 belonging to the La_2Ni_4 and the LaNi_5 sub-units, respectively. The observed spectra were well reproduced by simulated spectra [green and blue lines in Fig. 2(a)] from the simple nuclear spin Hamiltonian with $\nu_Q = 0.7$ MHz for green lines and $\nu_Q = 3.6$ MHz for blue lines. The value of $\nu_Q \sim 3.6$ MHz for one of the La sites was nearly temperature independent which was confirmed by the observation of NQR spectra as discussed below. In order to assign the La sites, we have calculated the electric field gradient at each La site by a full potential linear augmented plane wave (FLAPW) method [21] with a generalized gradient approximation [22] using the lattice parameters described in Introduction. The ν_Q values were calculated to be 0.5 MHz and 4.1 MHz for La1 and La2, respectively, where V_{ZZ} is parallel to the c axis for both sites. The relatively large difference in the ν_Q values for those two La sites is consistent with the experimental results. Therefore we assigned the signals with $\nu_Q \sim 3.6$ MHz to La2 and those with $\nu_Q \sim 0.7$ MHz to La1. As shown at the bottom in Fig. 2(a), the observed spectra above $T = 100$ K are reproduced with $\theta = 90^\circ$. Since V_{ZZ} is parallel to the c axis, $\theta = 90^\circ$ indicates that the c axis of the small grains in the loosely packed sample is aligned perpendicular to the external magnetic field. This indicates that the magnetization parallel to the ab plane (M_{ab}) is greater than M parallel to the c axis (M_c) under $H \sim 7.4$ T above 100 K.

To check this, we measured the temperature dependences of $(M/H)_{ab}$ and $(M/H)_c$ under a magnetic field of $H = 7$ T whose results are shown in Fig. 2(b) [23]. Although the $(M/H)_{ab}$ and $(M/H)_c$ are nearly the same in the paramagnetic state in the scale of the figure, one can see a small difference between $(M/H)_{ab}$ and $(M/H)_c$ as shown in the inset of Fig. 2(b) where $\Delta M/H = (M/H)_{ab} - (M/H)_c$ is plotted as a function of temperature. $\Delta M/H$ changes the sign around 90 K where $(M/H)_{ab}$ is greater than $(M/H)_c$ above 90 K while $(M/H)_{ab}$ is less than $(M/H)_c$ below that temperature. The positive value of $\Delta M/H$ above 100 K is consistent with the NMR results. Therefore our NMR data show that the $\Delta M/H$ is enough to orient the grains of the powder samples along the magnetic field direction even though $\Delta M/H$ is relatively small. Since the rotation of the grains of the powder samples is due to a torque acting on each grain, and the condition for getting an oriented powder sample depends on the size of each grain, $\Delta M/H$, and so on, we do not discuss those quantitatively here.

Now back to the NMR spectra. With decreasing temperatures, each line becomes broader and the spacings of lines for each NMR spectrum below ~ 100 K become twice those in the spectra above that temperature as typically shown in the upper two panels of Fig. 2(a). Those spectra measured at 85 K and 70 K are well reproduced with $\theta = 0$ with the same ν_Q values for the two La sites (the T independent ν_Q is confirmed by NQR measurements shown below). This means that the c axis of the

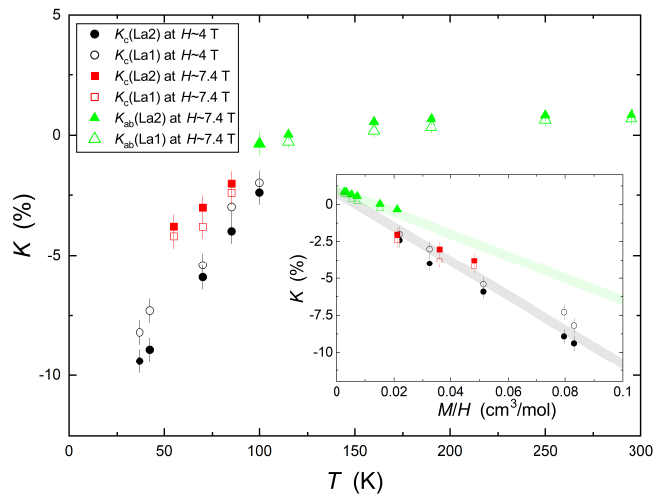


FIG. 3: Temperature dependence of the ^{139}La -NMR shifts: $^{139}K_{ab}$ (triangles) and $^{139}K_c$ (squares) at $H \sim 7.4$ T (red symbols below 100 K; green symbols above 100 K) and ~ 4 T (black symbols). Filled and open symbols correspond to La1 and La2, respectively. The inset shows the K vs. M/H plots for the corresponding H . Here we used M/H measured at 7 T for the K - M/H plot since no M/H data at 7.4 T are available [23]. The M/H data at 4 T are from Ref. [3]. The gray and green bold lines are the guides for the eye representing the slopes.

small grains of the powder sample is rotated by 90 degrees and now is oriented along the external magnetic field in that temperature range where M_c must be greater than M_{ab} . Again this is consistent with the negative values of $\Delta M/H$ below 90 K where $(M/H)_c$ is greater than $(M/H)_{ab}$ as seen in the inset of Fig. 2(b).

Figure 3 shows the temperature dependence of NMR shifts determined by the observed spectra. The filled and open symbols correspond to La1 and La2, respectively. The NMR shift data above 100 K correspond to the case for $H \parallel ab$ plane (K_{ab}) while $H \parallel c$ axis (K_c) below 100 K at $H \sim 7.4$ T. With decreasing temperature, the values of K for La1 and La2 decrease similarly. It is noted that the change in the slopes around 100 K is mainly due to the different values of the hyperfine coupling constants for the different magnetic field directions as described below. To see the effect of H on NMR shifts (or the magnetization), we also measured NMR spectra at a different magnetic field of $H \sim 4$ T whose results are shown by the black symbols in Fig. 3. As can be seen, the NMR shifts under ~ 4 T are greater than those at 7.4 T in magnitude. These observations are consistent with the T dependence of M/H under the different magnetic field where the M/H is suppressed with increasing H in the T range of $T = 50 - 100$ K [3].

The NMR shift consists of temperature dependent spin shift $K_s(T)$ and T independent orbital shift K_0 ; $K(T) = K_s(T) + K_0$ where $K_s(T)$ is proportional to the magnetization $M(T)$ divided by H , $M(T)/H$, via hyperfine

coupling constant A : $K_s(T) = \frac{A}{\mu_B N_A} \frac{M(T)}{H}$. Here N_A is Avogadro's number. Utilizing the T dependence of M/H in corresponding magnetic fields for the NMR measurements, we plot all K_c data as a function of M/H in the inset of Fig. 3. Here, for K_c at $H \sim 7.4$ T, we used M/H data measured at 7 T since no M/H data at 7.4 T are available [23]. Within our experiment uncertainty, all data below 100 K are roughly on lines as shown by the bold gray line, although the K_c data at 7.4 T seem to deviate slightly from the line. Since the M/H is sensitive to H at low temperatures [3], the deviation could be due to the different magnetic fields. From the slope of the gray line, we estimate the hyperfine coupling constants to be $A_c = -4.5 \text{ T}/\mu_B$ for $H \parallel c$ for both La sites without any clear difference between them within our experiment uncertainty. It is noted that the coupling constant estimated here is considered to be a total hyperfine coupling constant produced by the nearest neighboring (NN) Ni ions, as both La1 and La2 are surrounded by six NN Ni ions [24].

We also plotted the K_{ab} data (green symbols) as a function of $(M/H)_{ab}$ at 7 T in the inset of Fig. 3. Since M/H is less sensitive to H at high temperatures, it will be reasonable to estimate the hyperfine coupling constant along the ab plane (A_{ab}) even though the magnetic fields for the K_{ab} and M/H measurements are slightly different. From the slope of the bold green line, we obtained $A_{ab} = -3.0 \text{ T}/\mu_B$ for $H \parallel ab$ for both La sites.

B. ^{139}La NMR in the magnetically ordered states

Figures 4(a)-(c) show frequency-swept ^{139}La -NMR spectra in magnetically ordered states at $T = 4.3$ K for the loosely packed powder sample under magnetic fields of (a) 2 T, (b) 3.5 T, and (c) 8 T. As observed in the paramagnetic state, the spectra are the sum of the two sets of La NMR lines originating from La1 and La2 with $\nu_Q = 0.7$ MHz and 3.6 MHz, respectively. Since the observed spectra are relatively sharp and not so-called powder patterns, the small grains of the powder sample are also found to orient due to H , similar to the case of the NMR spectra in the paramagnetic state discussed in III. A. At $H = 2$ T, the observed spectrum was well reproduced by a sum of the two spectra from La1 (green hatched area) and La2 (light blue hatched areas) with $\theta = 90^\circ$ where we had to add the internal magnetic induction (B_{int}) at the La sites produced by Ni-ordered moments in the AFM state. Here we used $B_{\text{int}} = -0.37$ T (for La1) and -0.76 T (for La2) whose directions are parallel to the c axis as directly determined by the NQR spectra in the next subsection III. C. $\theta = 90^\circ$ indicates that the c axis of the small grains is perpendicular to the H due to the magnetization M_{ab} being greater than M_c in the AFM state (A phase) where the Ni ordered moments are perpendicular to H . This is consistent with the M data ($T = 5$ K) [3] shown in the inset of Fig. 4(a) where M_{ab} is greater than M_c for H less than ~ 6.2 T. A

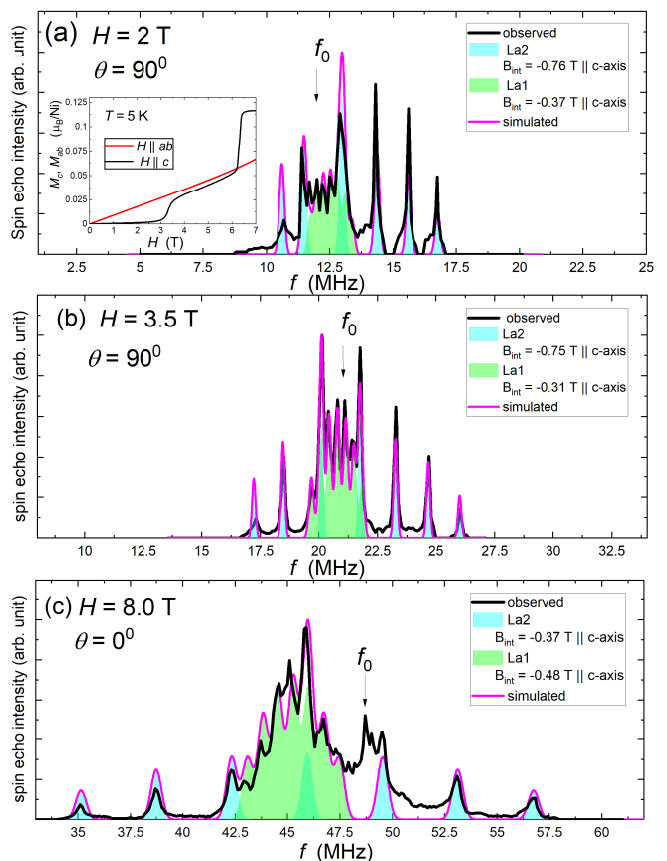


FIG. 4: Frequency-swept ^{139}La -NMR spectra at $T = 4.3$ K on the loosely packed powder sample under magnetic fields of (a) 2 T, (b) 3.5 T, and (c) 8 T. The green and blue curves are simulated spectra with $\nu_Q = 0.7$ MHz for La1 and $\nu_Q = 3.6$ MHz for La2, respectively, and different internal magnetic inductions B_{int} discussed in the text. The magenta curves are the sum of the two simulated spectra. The down arrows (f_0) correspond to the Larmor frequencies for each magnetic field. The peak around f_0 clearly observed in the spectrum at $H = 8$ T probably comes from impurities. The inset of (a) shows the external magnetic field dependence of M for $H \parallel ab$ (M_{ab} in red) and $H \parallel c$ (M_c in black) measured at 5 K from Ref. [3].

similar spectrum with $\theta = 90^\circ$ was observed at $H = 3.5$ T with a similar set of the parameters of $B_{\text{int}} = -0.31$ T and -0.75 T for La1 and La2, respectively, with the same ν_Q values. On the other hand, when the system sets in a saturated paramagnetic state under $H = 8$ T, the spectra become wider due to the change in θ from 90° to 0° . This corresponds to the c axis of the small grains of the powder sample oriented along H , which is again consistent with the M data where M_c is now greater than M_{ab} above $H \sim 6.2$ T. From the fit of the spectra with keeping the same ν_Q values for each La site, we found that B_{int} is parallel to the c as well and those values are -0.48 T and -0.37 T for La1 and La2, respectively.

Utilizing the hyperfine coupling constant $A_c = -4.5 \text{ T}/\mu_B$, $B_{\text{int}} = -(0.31-0.37)$ T for La1,

and $-(0.76-0.75)$ T for La2, we estimated the average values of Ni ordered moments around La1 and La2 to be $\sim 0.07-0.08 \mu_B$ and $\sim 0.17 \mu_B$, respectively, in the AFM state (A phase). The average value of Ni-ordered moments around La1 is nearly half of that around La2, suggesting a nonuniform distribution of the Ni-ordered moments in the AFM state. This is qualitatively consistent with the AFM state predicted by the theory and the ND measurement, where the maximum amplitude of the Ni-ordered moments is expected at the middle of two LaNi_5 sub-units close to La2 while the minimum amplitude of the Ni-ordered moments is proposed at Ni ions in the La_2Ni_4 sub-unit close to La1.

We also estimate the average values of Ni-ordered moments to be $\sim 0.11 \mu_B$ and $\sim 0.08 \mu_B$ around La1 and La2, respectively, in the saturated paramagnetic state. According to the theoretical calculations, in the ferromagnetic state, the ferromagnetic units are stacked ferromagnetically while keeping the nonuniform distribution of the moments as in the AFM state [10]. In this case, we expect almost no change in the average values of Ni-ordered moments around both La sites in the saturated paramagnetic state as compared to the AFM state. This is inconsistent with the NMR results showing that the average values of Ni-ordered moments are more uniformly distributed in Ni positions than the case of AFM state.

C. ^{139}La NQR spectrum

At zero magnetic field, the electric quadrupole Hamiltonian (the second term of Eq. 1) for the case of $I = 7/2$ produces three equally spaced NQR lines at resonance frequencies of ν_Q , $2\nu_Q$, and $3\nu_Q$ corresponding to the transitions of $m = \pm 1/2 \leftrightarrow \pm 3/2$, $\pm 3/2 \leftrightarrow \pm 5/2$ and $\pm 7/2 \leftrightarrow \pm 5/2$, respectively. From NMR measurements, the values of ν_Q are estimated to be ~ 3.6 MHz for La2, so one expects three NQR lines at 3.6 MHz, 7.2 MHz, and 10.8 MHz, named ν_1 , ν_2 , and ν_3 lines, respectively. In fact, we observed such NQR lines in the paramagnetic state as shown in Fig. 5(a) where the ν_1 line was not measured due to the limitation of the resonance frequency of our spectrometer (we also could not measure the NQR lines for the La1 site due to the small value of $\nu_Q \sim 0.7$ MHz). The observed NQR spectra, that is, the peak frequencies for the ν_2 and ν_3 lines for the La2 site are well reproduced with $\nu_Q = 3.63$ MHz as shown by the calculated spectra in magenta, and those peak frequencies are independent of temperature in the paramagnetic state [see Fig. 5(b)], indicating no change of ν_Q with temperature.

In the AFM state, we found that each line splits into two lines, as shown in Fig. 5(a). This is due to the appearance of B_{int} at La2 produced by Ni-ordered moments in the AFM state where B_{int} lifts the degenerate nuclear spin levels of $\pm m$ states. To estimate B_{int} , we calculated NQR spectra using a Hamiltonian where a Zeeman term

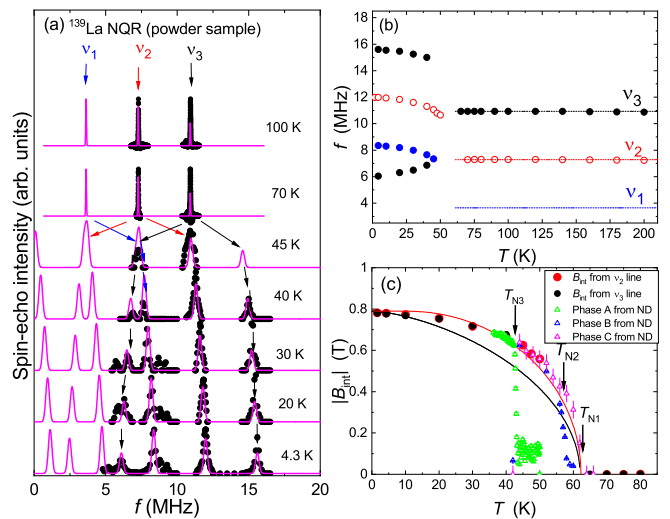


FIG. 5: (a) ^{139}La NQR spectra for La2 at zero magnetic field at various temperatures in both the paramagnetic and magnetic ordered states. The magenta curves are simulated spectra. (b) Temperature dependence of the resonance frequency for each peak. The symbols in black, red and blue represent for ν_3 , ν_2 and ν_1 lines, respectively. (c) Temperature dependence of the magnitude of the internal magnetic induction ($|B_{\text{int}}|$) at La2. The black circles are estimated B_{int} from the ν_3 line and the red circles are from the ν_2 line. The expected temperature dependences of B_{int} based on the ND data [4] are also plotted in (c) by the green open triangles (the c components of the ordered moments in the commensurate antiferromagnetic A phase), the blue open triangles (the c components of the ordered moments in the incommensurate antiferromagnetic B phase), and the magenta open triangles (the ab plane components of the ordered moments in the incommensurate antiferromagnetic B and C phases). The ND data sets shown by the green, blue, and magenta symbols were normalized to scale the NMR data at 40 K, 45 K, and 50 K, respectively. The black and red curves show the typical temperature dependence of B_{int} based on the SCR theory and the localized moments picture, respectively (see text).

due to B_{int} , similar to the first term of Eq. 1, was added to the electrical quadrupole Hamiltonian. We found that the observed spectra were well reproduced by taking B_{int} parallel to the c axis, as shown by the calculated spectra in magenta in the magnetically ordered state. The value of $|B_{\text{int}}| \sim 0.79$ T at 4.3 K is close to the values of $-(0.76-0.75)$ T estimated from the NMR spectrum in the A phase. The temperature dependence of B_{int} at the La2 site is shown in Fig. 5(c), which corresponds to the temperature dependence of sublattice magnetization M_{sub} . Here we also plotted the expected temperature dependence of M_{sub} ($\propto B_{\text{int}}$) based on the ND data [4] in the commensurate antiferromagnetic A phase (the c components of the ordered moments by green open triangles), the incommensurate antiferromagnetic B phase (the c components by blue open triangles), and the incommensurate antiferromagnetic B and C phases (the ab plane components by magenta open triangles). The ND

data sets shown by the green, blue, and magenta symbols were normalized to scale the NMR data at 40 K, 45 K, and 50 K, respectively. It is noted that the phase transitions at T_{N2} and T_{N1} are of second order while the first order phase transition was observed at T_{N3} [4]. It is also noted that the temperature dependences of M_{sub} from the ND measurements in the magnetically ordered states are well overlapped with that of B_{int} determined by the NMR measurements although the overlapped temperature range ($T = 35 - 50$ K) is not wide.

According to self-consistent renormalization (SCR) theory, the temperature dependence of M_{sub} for the case of weak itinerant antiferromagnets, the temperature dependence of M_{sub} is given by [25]

$$M_{\text{sub}}(T) \propto \sqrt{1 - (T/T_N)^{3/2}} \quad (3)$$

The black curve is the calculated temperature dependence of $|B_{\text{int}}|$ ($=B_{\text{int},0}\sqrt{1 - (T/T_N)^{3/2}}$) based on the above formula with $B_{\text{int},0} = 0.79$ T and $T_N = 62$ K, which does not reproduce the experimental data well. Since the phase transition at T_{N3} is of first order, we also tried to fit only for the data above T_{N3} using the formula. However, we could not fit the data well with a reasonable value of $B_{\text{int},0}$. In addition, it is clear that the observed temperature dependence of B_{int} cannot be explained by the formula using the different values of T_N . Thus we conclude that the temperature dependence of the M_{sub} in La_2Ni_7 cannot be explained by the model of weak itinerant antiferromagnets. Instead, the temperature dependence of B_{int} was found to be reasonably reproduced by a Brillouin function which was calculated based on the Weiss molecular field model shown by the red curve where we tentatively assumed $S = 1$ and used $T_N = 62$ K. Here we normalized the calculated temperature dependence to scale with $|B_{\text{int}}|$ at the lowest temperature. These results may indicate that the magnetic state of the Ni ions is more likely described by the local-moment picture, contrary to the anticipation from the small Ni-ordered moments in the itinerant antiferromagnet La_2Ni_7 . Interestingly, similar discrepancy between M_{sub} and the SCR theory has been reported in weak itinerant antiferromagnets such as V_5Se_8 [26], V_5S_8 [27], CrB_2 [28], and YMn_{12} [29].

The direction of B_{int} in the AFM state is also directly confirmed by ^{139}La NQR spectrum measurements on the single crystal in nonzero H . Figure 6 shows the H dependence of NQR spectrum at 1.6 K under small magnetic fields applied parallel to the c axis using a single crystal. With the application of small H less than 0.2 T, we found that one of the split ν_2 lines that is shifted to higher frequency side (around 12 MHz) further splits into two lines as shown in Fig. 6. Similar splitting is also observed for the ν_3 line around 15.6 MHz under small magnetic fields. These results clearly indicate the existence of two La_2 sites with B_{int} parallel or antiparallel to the c axis. Since the effective field at the La site is given by the vector sum of \mathbf{B}_{int} and \mathbf{H} , i.e., $|\mathbf{B}_{\text{eff}}| = |\mathbf{B}_{\text{int}} + \mathbf{H}|$, the resonance

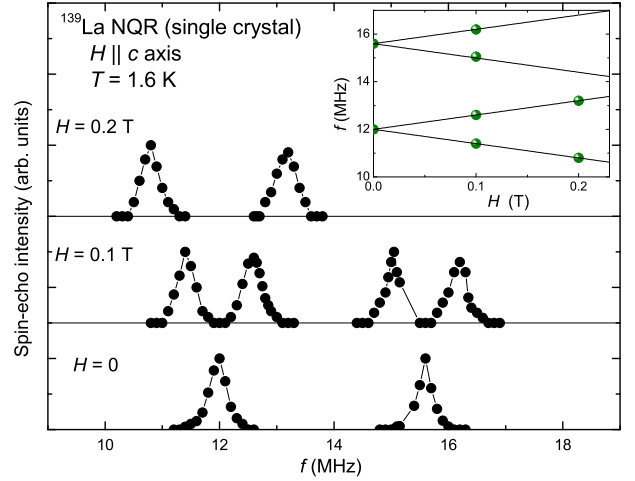


FIG. 6: ^{139}La NQR spectra for La_2 under small magnetic fields at 1.6 K. The inset shows the external magnetic field dependence of peak frequencies of the split lines for the ν_2 and ν_3 lines. The solid lines are the expected H dependence of peak frequencies when B_{int} is parallel or antiparallel to the c axis.

frequency is expressed for $H \parallel B_{\text{int}}$ as $f = \frac{\gamma_N}{2\pi}|B_{\text{eff}}| = \frac{\gamma_N}{2\pi}|B_{\text{int}} \pm H|$. As shown in the inset, the H dependence of the split peak frequencies is well reproduced by the relation using the $\frac{\gamma_N}{2\pi} = 6.0146$ MHz/T for La nucleus, evidencing that the B_{int} is parallel or antiparallel to the c axis without any obvious deviation. This result also clearly shows the appearance of two sublattices, a direct confirmation of the antiferromagnetic state.

To see how the NQR spectra change around magnetic phase transition temperatures for the investigation of the AFM states of the B and C phases, we measured the NQR spectra around 11 MHz at zero magnetic field for the three phases. Figure 7 shows the measured NQR spectra for the powder samples in the three magnetic phases together with the one in the PM state. The line around 10.9 MHz in the PM state corresponds to the ν_3 line. When the sample is in the AFM state at $T = 58$ K (C phase), we found that the position of the NQR line does not change, although the line becomes slightly broad. This could be explained by (1) very small B_{int} in the phase and/or (2) B_{int} points perpendicular to the c axis. According to the ND measurements, the C phase is proposed as an incommensurate AFM state with the Ni-ordered moment perpendicular to the c axis. Our NQR spectrum in the C phase would be not inconsistent with the ND data. With the further decrease in temperature, the signal around 10.9 MHz disappeared when the system entered the B phase (for example, see the NQR line at $T = 50$ K). Instead, we observed the slightly broader NQR line centered at 10.5 MHz, lower than the peak frequency of 10.9 MHz in the paramagnetic state and the C phase. We assigned the line to be one of the split ν_2 lines due to B_{int} along the c axis because the position of the

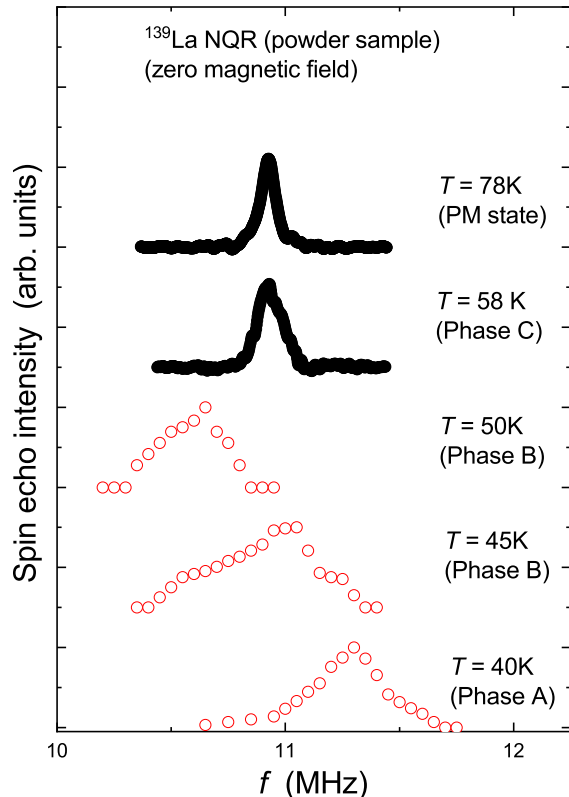


FIG. 7: ^{139}La NQR spectra for La2 at zero magnetic field at various temperatures in both the paramagnetic and the magnetically ordered states. The spectra shown by black solid and red open circles are the ν_3 and ν_2 lines, respectively.

line smoothly connects to that of the line in the A phase [see Fig. 5(c)]. This suggests that the dominant component of the B_{int} at La2 is parallel or antiparallel to the c axis in the B phase, similar to the case in the A phase. According to the ND data, the incommensurate propagation vector is along the c axis in the B phase, which indicates that the Ni ordered moments are no longer ferromagnetic block [4]. In this case, one expects the large distribution of B_{int} at the La sites. Therefore the NMR data would be inconsistent with the ND results. The slightly broader lines are due to small distributions of B_{int} . This suggests slight distributions of the Ni-ordered moments in the B phase, but probably not due to the incommensurate AFM state reported from the ND data. In contrast, as we discussed in the previous subsection, the commensurate AFM state (Phase A) reported from the ND measurements is consistent with the NMR results.

D. ^{139}La spin-lattice relaxation time T_1

Figure 8 shows the T dependence of $1/T_1T$ at the ν_3 line of ^{139}La NQR spectrum under zero magnetic field. In the paramagnetic state, $1/T_1T$ is nearly constant above 150 K and starts to increase below that temperature with

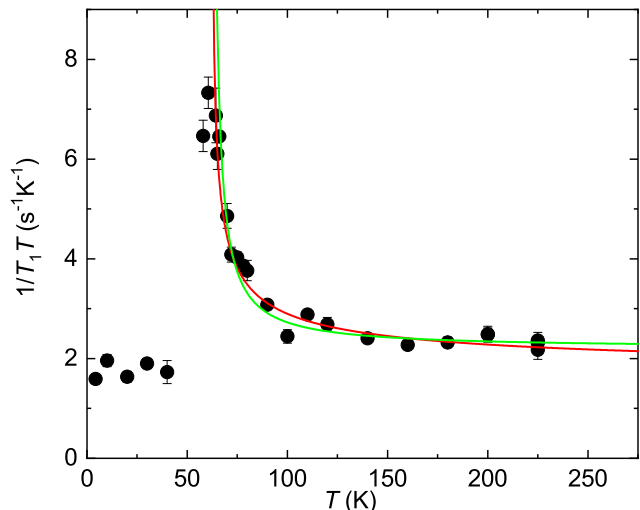


FIG. 8: Temperature dependence of $1/T_1T$ measured at the $3\nu_Q$ line in the paramagnetic and magnetic states. The red and green curves are the calculated results based on the SCR theory and the localized moments picture, respectively (see text).

decreasing T , and shows a peak around T_{N1} due to critical slowing down of spin fluctuation, characteristics of second order phase transition. In the AFM state (A phase), the $1/T_1T = \text{constant}$ behavior expected for metals is observed, consistent with the itinerant nature of La_2Ni_7 .

Since the compound has small ordered moments, we first fit the data based on the SCR theory. For the case of weak itinerant antiferromagnets, the SCR theory predicts the temperature dependence of $1/T_1T$ in paramagnetic states given by [30, 31]

$$1/T_1T = \frac{a}{\sqrt{T - T_N}} + b \quad (4)$$

where the first term originates from AFM fluctuations around a wave vector $q = Q$ (Q being antiferromagnetic wave vector) and the second term is due to Korringa-type relaxation, a characteristic feature of metallic materials. The red curve in the paramagnetic state shows the calculated results based on the SCR theory with a set of parameters of $a = 8 \text{ (s}^{-1}\text{K}^{-0.5}\text{)}$, $b = 1.6 \text{ (s}^{-1}\text{K}^{-1}\text{)}$ and $T_N = 62 \text{ K}$, which reproduces the experimental data in contrast to the case of the T dependence of B_{int} .

On the other hand, as the T dependence of B_{int} suggests the localized moment nature rather than the weak itinerant antiferromagnets, we also analyzed the T_1 data with the localized moment model described by

$$1/T_1T = \frac{a'}{T - \Theta} + b' \quad (5)$$

where the first term originates from the paramagnetic uniform spin fluctuations of localized spins described by

Curie-Weiss behavior of the magnetic susceptibility, i.e., $1/T_1 \propto \chi T$ and the second term is Korringa-type relaxation, a characteristic feature of metallic materials as in eq. 4. With $a' = 20$ (s^{-1}), $b' = 2.2$ ($\text{s}^{-1}\text{K}^{-1}$), and $\Theta = 62$ K, the experimental data are also reproduced reasonably well as shown by the green curve in Fig. 8. Therefore, both the SCR theory and the localized moment model can explain the observed T dependence of $1/T_1$, although those are different in character of spin fluctuations. Thus, given the small Ni-ordered moments evidenced by the magnetization and present NMR spectrum measurements, our experimental results suggest that La_2Ni_7 has both the characteristic natures of weak itinerant and localized moment antiferromagnets.

IV. SUMMARY

In summary, we have carried out the microscopic characterization of the itinerant antiferromagnet La_2Ni_7 by ^{139}La NMR and NQR measurements. Our results suggest the presence of commensurate antiferromagnetic A phase with Ni ordered moments aligned along crystalline c axis. Furthermore, a non-uniform distribution of the Ni-ordered moments was found with the comparative analysis of inequivalent La1 and La2 sites. In the saturated paramagnetic state under a magnetic field of 8 T

at 4.3 K, the Ni-ordered moments were found to become more uniform. The temperature dependence of the sublattice magnetization measured by the internal magnetic induction B_{int} at the La2 site is reproduced by the local moment model. The temperature dependence of ^{139}La spin-lattice relaxation time (T_1) suggests that the paramagnetic to antiferromagnetic phase transition at T_{N3} is second order in nature and its temperature dependence in the paramagnetic state can be well produced by both the local moment and the self-consistent renormalization model for weak itinerant antiferromagnets. Our NMR results revealed a peculiar magnetism in the itinerant antiferromagnet La_2Ni_7 that exhibits the properties of both localized and itinerant nature.

V. ACKNOWLEDGMENTS

The authors would like to thank J. Wilde for providing the neutron diffraction data and also for fruitful discussions. The research was supported by the U.S. Department of Energy, Office of Basic Energy Sciences, Division of Materials Sciences and Engineering. Ames National Laboratory is operated for the U.S. Department of Energy by Iowa State University under Contract No. DE-AC02-07CH11358.

-
- [1] P. C. Canfield and S. L. Bud'ko, Rep. Prog. Phys. **79**, 084506 (2016).
- [2] P. C. Canfield, Rep. Prog. Phys. **83**, 016501 (2020).
- [3] R. A. Ribeiro, S. L. Bud'ko, L. Xiang, D. H. Ryan, and P. C. Canfield, Phys. Rev. B **105**, 014412 (2022).
- [4] J. M. Wilde, A. Sapkota, W. Tian, S. L. Bud'ko, R. A. Ribeiro, A. Kreyssig, and P. C. Canfield, Phys. Rev. B **106**, 075118 (2022).
- [5] K. Lee, N. H. Jo, L-L Wang, R. A. Ribeiro, Y. Kushnirenko, B. Schruck, P. C. Canfield, A. Kaminski, arXiv:2205.09211
- [6] A. V. Virkar and A. Raman, J. Less Comm. Met. **18**, 59 (1969).
- [7] K.H.J. Buschow and A.S. Van Der Goot, J. Less Comm. Met. **22**, 419 (1970).
- [8] The crystal structure was drawn by using VESTA [K. Momma and F. Izumi, J. Appl. Crystallogr. **44**, 1272 (2011)].
- [9] V. Paul-Boncour, J.- C. Crivello, N. Madern, J. Zhang, L.V.B. Diop, V. Charbonnier, J. Monnier, M. Latroche, J. Phys.: Condens. Matter, **32**,415804 (2020).
- [10] J.-C. Crivello and V. Paul-Boncour, J. Phys.: Condens. Matter **32**, 145802 (2020).
- [11] K. H. J. Buschow, J. Mag. Mag. Mater. **40**, 224 (1983).
- [12] F. T. Parker and H. Oesterreicher, J. Less Comm. Met. **90**, 127 (1983).
- [13] Y. Tazuke, R. Nakabayashi, S. Murayama, T. Sakakibara, and T. Goto, Phys. B: Condens. Matter **186-188**, 596 (1993).
- [14] M. Fukase, Y. Tazuke, H. Mitamura, T. Goto, and T. Sato, Mater. Trans., JIM **41**, 1046 (2000).
- [15] M. Fukase, Y. Tazuke, H. Mitamura, T. Goto, and T. Sato, J. Phys. Soc. Jpn. **68**, 1460 (1999).
- [16] Y. Tazuke, H. Suzuki, and H. Tanikawa, Phys. B: Condens. Matter **346-347**, 122 (2004).
- [17] For example, Q.-P. Ding, N. S. Sangeetha, W. R. Meier, M. Xu, S. L. Bud'ko, P. C. Canfield, D. C. Johnston, and Y. Furukawa, Phys. Rev. B **102**, 180406(R) (2020); Q.-P. Ding, W. R. Meier, J. Cui, M. Xu, A. E. Böhrer, S. L. Bud'ko, P. C. Canfield, and Y. Furukawa, Phys. Rev. Lett. **121**, 137204 (2018); Q.-P. Ding, N. Higa, N. S. Sangeetha, D. C. Johnston, and Y. Furukawa, Phys. Rev. B **95**, 184404 (2017); Q.-P. Ding, P. Wiecki, V. K. Anand, N. S. Sangeetha, Y. Lee, D. C. Johnston, and Y. Furukawa, Phys. Rev. B **93**, 140502(R) (2016).
- [18] D. E. MacLaughlin, J. D. Williamson, and J. Butterworth, Phys. Rev. B **4**, 60 (1971).
- [19] C. P. Slichter, *Principles of Magnetic Resonance*, 3rd ed. (Springer, New York, 1990).
- [20] Here we omitted in the quadrupole Hamiltonian a term containing the asymmetry parameter η of the electric field gradient since it is found to be zero from NQR experiment and also the DFT calculation.
- [21] P. Blaha, K. Schwarz, G. K. H. Madsen, D. Kvasnick, and J. Luitz, WIEN2K, An Augmented Plane Wave+Local Orbitals Program for Calculation Crystal Properties (Karlheinz Schwarz, Technical Universität Wien, 2001).
- [22] J. P. Perdew, K. Burke, and M. Ernzerhof, Phys. Rev. Lett. **77**, 3865 (1996).
- [23] The magnetization measurements were performed with a

- Quantum Design Magnetic Properties Measurement System (MPMS). Due to the limitation of the magnetic field of our MPMS, the magnetization was measured at 7 T, the highest magnetic field of the MPMS.
- [24] In addition to the 6 NN Ni ions for the La1 and La2 sites, there are 3 second NN and 3 third NN Ni ions for the La1 site and 6 second NN and 6 third NN Ni ions for the La2 site.
 - [25] H. Hasegawa and T. Moriya, *J. Phys. Soc. Jpn.* **36**, 1542 (1974).
 - [26] Y. Kitaoka and H. Yasuoka, *J. Phys. Soc. Jpn.* **48**, 1460 (1980).
 - [27] Y. Kitaoka and H. Yasuoka, *J. Phys. Soc. Jpn.* **48**, 1949 (1980).
 - [28] Y. Kitaoka and H. Yasuoka, *J. Phys. Soc. Jpn.* **49**, 493 (1980).
 - [29] K. Yoshimura, H. Yasuoka, and Y. Nakamura, *J. Magn. Mater.* **90-91**, 706 (1990).
 - [30] T. Moriya, *Spin Fluctuations in Itinerant Electron Magnetism*, Vol. 56 (Springer-Verlag, 1985).
 - [31] T. Moriya and K. Ueda, *Solid State Commun.*, **15**, 169 (1974).